

# Influence of the Intraday Electricity Market Structure on the Degradation of Li-Ion Batteries Used to Firm Photovoltaic Production

Hector Beltran, Pablo Ayuso, Javier Cardo-Miota, Jorge Segarra-Tamarit, Néstor Aparicio, and Emilio Pérez\*

This article considers the introduction of Li-ion batteries in photovoltaic power plants to firm their energy production and analyzes the dependence of their degradation on the structure of the electricity market where the power production is traded. The operation of the batteries is decided as a result of successive optimization problems that benefit from the use of deep-learning-based irradiance forecasting tools with low prediction error, which allows the batteries to keep a small size. In addition, state-of-the-art battery aging models are handled to derive a realistic lifetime prognosis. The simulation results obtained by using real data from three European locations, which have different irradiance patterns and market structures, show how the proposed control strategy makes it possible to decouple the saturation rate of the batteries from the climatic conditions of the plant location. Furthermore, regarding the market structure, the results show that the shorter the energy block and the closer the lead time, the lower is the degradation of the batteries.

important wind power penetration, will impact the grid stability and operation.<sup>[2]</sup> Given that the pace of updating the interconnection infrastructure among control areas, which would allow greater power exchanges, is limited, transmission system operators (TSOs) need to rely on alternative solutions, such as energy storage systems (ESS), to balance the system. In this sense, one technology stands out: lithium-ion (Li-ion) batteries. This is due to the tenfold downward trend in per kilowatt hour cost experienced by commercial battery packs in the last 10 years.<sup>[3,4]</sup> If the evolution of the PV industry is mimicked, the trend toward cheaper batteries is expected to continue in the coming years. This consolidates Li-ion batteries as a key player in the future electricity grid, primarily in combination with PV installations. The level-


## 1. Introduction

Worldwide growth of photovoltaics (PV) has been exponential during the last 15 years with a global installed capacity skyrocketing from hardly 1 GW in 2006 to more than 620 GW in 2019.<sup>[1]</sup> Further deployment seems unstoppable because of the sustained decline in utility-scale solar PV electricity cost experienced so far, which has transformed solar PV plants into one of the cheapest electricity supplies.

The introduction of such a massive quantity of intermittent nondispatchable generation, complemented by the also

ized cost of electricity for large PV plants integrating a 4 h capacity battery energy storage system (BESS) is between \$85 and \$158 per MWh, rapidly decreasing year after year.<sup>[5]</sup> This production cost starts making these hybrid plants competitive when they provide grid services such as frequency and voltage control, inertia emulation, output smoothing, and peak shaving.<sup>[6]</sup> In the US market, batteries are allowed to provide these services, which are remunerated to complement the generation income.<sup>[7]</sup> The European scenario, however, is quite the opposite nowadays and still presents a variety of national and regional legislations that, combined with government auctions that tend to undervalue storage, do not favor the introduction of ESS. This trend would be starting to change with the progress of the unifying process of the European electricity sector with initiatives like PICASSO<sup>[8]</sup> and MARI.<sup>[9]</sup> These projects try to set up a joint European platform for the exchange of balancing energy from frequency restoration reserves with automatic and manually activation, respectively. Therefore, it opens the door to a favorable and widespread policy frame inciting the deployment of these types of installations via a proper service remuneration. In the same way, the Recovery and Resilience Facility derived from the pandemic situation allows the European Commission to raise funds (723.8 billion €) to help member states implement reforms and investments that are in line with the priorities of the European Union (EU).<sup>[10]</sup> It concentrates important amounts

H. Beltran, P. Ayuso, J. Cardo-Miota, J. Segarra-Tamarit, N. Aparicio, E. Pérez  
Area of Electrical Engineering  
Universitat Jaume I  
12071 Castelló de la Plana 12071, Spain  
E-mail: pereze@uji.es

 The ORCID identification number(s) for the author(s) of this article can be found under <https://doi.org/10.1002/ente.202100943>.

© 2022 The Authors. Energy Technology published by Wiley-VCH GmbH. This is an open access article under the terms of the Creative Commons Attribution-NonCommercial License, which permits use, distribution and reproduction in any medium, provided the original work is properly cited and is not used for commercial purposes.

DOI: 10.1002/ente.202100943

to boost the green transition, including BESS installations, in line with EU's 2030 climate ambition.

Beyond the industry involved, academics have also devoted attention to these types of installations. Three topics receive outstanding research in this context: the size and operation of the batteries, the forecast of the PV production, and the degradation of the batteries involved. For the first of them, multiple analyses have been lately performed to define the optimal size of BESS installed in PV plants targeting various goals.<sup>[11]</sup> For instance, Monteiro et al.<sup>[12]</sup> studied the optimal placement and sizing of BESS at the distribution grid level. Nasrolahpour et al.<sup>[13]</sup> did the same but sizing BESS from a market integration perspective. Concurrently, other references focus on control strategies developed to drive PV plants with BESS targeting to provide different services such as power ramp-rate control,<sup>[14]</sup> or secondary reserve,<sup>[15]</sup> to mitigate grid congestion from high surplus PV power feed-in,<sup>[16]</sup> or to improve the integration of EV and PV systems at the distribution level.<sup>[17]</sup> Still, Abdelrazek and Kamalasadani<sup>[18]</sup> introduced a remarkable work on PV capacity firming combined with a time shifting of the production; Wang et al.<sup>[19]</sup> discussed the PV capacity firming operation with 5 min power steps; and Pantos et al.<sup>[20]</sup> analyzed similar operation but considering dispersed ESS. For all these proposals, it becomes critical to use an accurate irradiance forecasting technique such as those based on deep-neural networks (DNN).<sup>[21]</sup> This allows to generate proper constant by periods production commitments to be traded in the corresponding electricity markets and avoid yielding committed energy deviations.<sup>[22]</sup> Finally, works involving the analysis of the batteries degradation when these are implemented in PV plants (for different goals) are also found in the literature. For instance, Beltran et al.<sup>[14]</sup> analyzed the aging when the batteries are providing ramp rate control to the PV production. Others analyze the degradation when batteries are used to provide ancillary services,<sup>[23]</sup> energy arbitrage,<sup>[24]</sup> or peak shaving.<sup>[25]</sup> Therefore, the degradation of the batteries is a hot topic in this field and a key parameter in the profitability analyses of hybrid plants. Altogether, although references can be identified in the literature with titles specifically concerning the use of batteries to firm the production of large PV plants,<sup>[26,27]</sup> none of the works published so far analyzed the influence of the electricity market structure on the aging of the batteries used for PV firming. This is the main contribution successfully developed in this work. This article analyzes how the degradation of the optimally sized batteries varies depending on the market where the hybrid plant is operated. To this end, the work uses a low prediction error deep-learning-based irradiance forecasting tool that favors the adoption of the minimum-sized batteries required to firm the PV production. Also, state-of-the-art battery aging models for both NMC and LFP Li-ion battery types are implemented. Results at three different European locations offer realistic lifetime calculations under the most typical European intraday market configurations.

The article is organized as follows: Section 2 introduces both the different European electricity intraday markets and the semiempirical aging models taken as framework for the BESS degradation analysis. In Section 3, the control methodology implemented to firm the production of PV plants with BESS is presented. Section 4 introduces the simulations

performed, and analyzes the results obtained under the described control methodology and the various market structures considered, in terms of required battery sizes and lifetime expectancy. Finally, the conclusions are presented in Section 5.

## 2. PV Plant Operation Context and Battery Aging Models

### 2.1. Intraday Market Structures under Analysis

PV installations including batteries are gaining momentum around the world. Most of these hybrid projects rely on trading their energy production in bilateral contracts. However, merchant options are attracting investors' interest. The economics of these projects remain highly dependent on the location, due to the electricity market to which the plant will be subject, and to the policy conditions associated with it. This implies the necessity to carefully analyze the economic viability for each project. Different market and policy contexts are faced across the Atlantic.

On the one hand, while the Federal Energy Regulatory Commission (FERC) strives through Order No. 841<sup>[28]</sup> to establish standards for the participation of energy storage in wholesale markets throughout the US, the existence of six different Independent System Operators is introducing some barriers to the homogenization procedure. This poses difficulties for a general study on the intraday market opportunities for storage installations in the US. On the other hand, the EU initiated the integration procedure of electricity markets about 15 years ago with the formation of various regional market areas (MAs), as shown in **Figure 1**. Nowadays, these MAs run together at the daily and the intraday level. In this sense, the daily markets of eight European power exchanges have been coupled since 2013 using a common clearing algorithm called the Pan-European Hybrid Electricity Market Integration Algorithm (EUPHEMIA).<sup>[29]</sup> Similarly, the Cross-Border Intraday Project (XBID) has unified the intraday markets since 2018.<sup>[30]</sup>

The XBID system is a trading solution designed to enable power exchanges and energy contracts across the different European regional MAs in a continuous, transparent, and efficient way. Therefore, it enables both multiple exchanges within the different geographies and trading cross-border energy contracts continuously on a 24/7 basis. The variety of products supported by XBID is summarized in **Figure 1**. Note that the products are configured by MA within XBID. In this way, XBID includes 60 min blocks for all the MAs as well as 15 and 30 min blocks for some of them. The products must comply with a minimum volume size per increment of 0.1 MW, a price tick of 0.1 € per MWh, and a price range from −9,999 to 9,999 € per MWh. Also note in **Figure 1** how the lead times vary among MAs. The shortest delivery horizon (5 min) is defined in “Belgium and The Netherlands” for their hourly available products. Moreover, France, Austria, and Germany fix 30 min horizons in their products. For the rest of MAs, including all the cross-border exchanges, 60 min leads are implemented. Finally, the matching of contracts either locally or cross-border is always performed in compliance with the price-time-priority

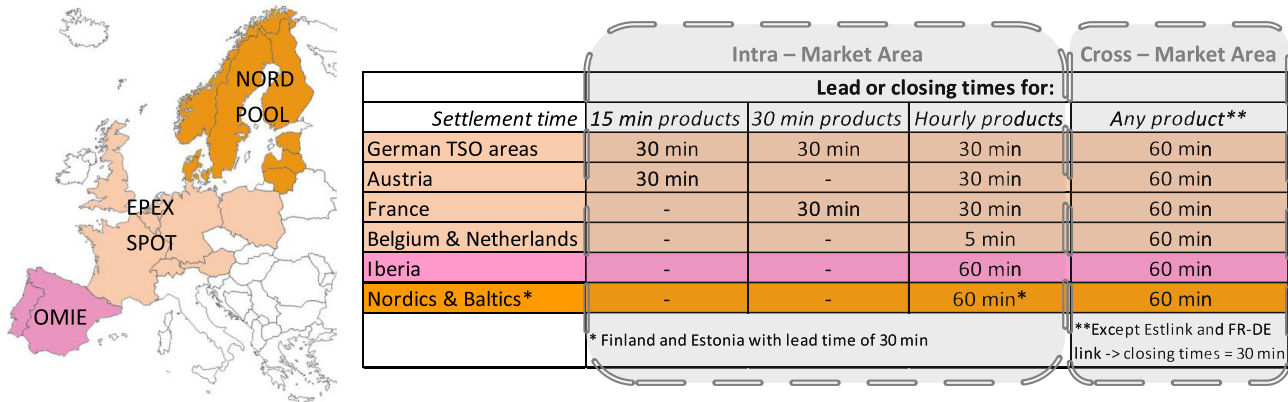


**Figure 1.** Lead times at the different MAs for the various products offered in the XBID.<sup>[31]</sup>

principle, while the XBID solution only enables the trading of contracts between MAs when enough interconnection capacity is available.

Apart from XBID, three complementary regional intraday markets operate in parallel with the common European market to cope with MA peculiarities or cross-border transfer limitations: one at the Iberian Market (MIBEL) between Portugal and Spain, and two more in Italy at the capacity calculation regions of “Greece–Italy” and “Italy–North”.<sup>[30]</sup> These markets are operated by means of just a series of discrete auctions in the intraday time frame (6 for MIBEL and 3 for the Italian regions) which not only improves the liquidity of the market but also increases the lead time and reduces the number of time windows when corrections can be introduced in the traded energy. Therefore, these types of markets do not favor the operation of PV plants with batteries for capacity firming. The increased difficulty of estimating the PV production as the delivery time gets further from the trading period favors the appearance of unexpected production biases. They usually involve economic penalties.

Among the various operation frameworks available for PV plants with batteries in the European context, the analysis introduced in this work focuses on the common XBID intraday market that currently runs across the continent and is available for all the European agents, that is, the daily and the different regional intraday markets are neglected. Therefore, the study analyzes the influence on the degradation of the batteries of the different combinations of XBID products summarized in Figure 1, with varying delivery periods and various lead times.

## 2.2. Degradation Models for Li-Ion Batteries

Li-ion batteries are the dominant technology in the energy storage sector nowadays because they clearly outperform other chemistries at a technical and economical level. Within the Li-ion battery industry there are six types of chemistries: lithium cobalt oxide (LiCoO<sub>2</sub>), lithium manganese oxide (LiMn<sub>2</sub>O<sub>4</sub>), lithium iron phosphate (LiFePO<sub>4</sub>), lithium, nickel, cobalt, and aluminum oxide (LiNiCoAlO<sub>2</sub>), lithium, nickel, manganese, and cobalt oxide (LiNiMn-CoO<sub>2</sub>), and lithium titanate (Li<sub>4</sub>Ti<sub>5</sub>O<sub>12</sub>). Being all commercial nowadays, two of them stand

out as the best fitted alternatives to operate in combination with renewable power plants<sup>[31]</sup>: LiFePO<sub>4</sub> (LFP) and LiNiMn – CoO<sub>2</sub> (NMC).

A great concern in such applications is the degradation experienced by the batteries as the power plant operates. The ability to estimate the aging in both real-time and forecasting future trends is crucial for a safe and effective use.<sup>[32]</sup> Diverse types of degradation models are available in the literature to predict the aging of the batteries.<sup>[33,34]</sup> These are usually classified into<sup>[35]</sup>: electrochemical models (detail and model the phenomena occurring into the battery),<sup>[36,37]</sup> equivalent circuit-based models (the battery is reduced as an equivalent circuit model),<sup>[38–40]</sup> analytical or semiempirical models with empirical fitting (estimation of aging parameters through measurements),<sup>[41–43]</sup> and statistical approaches or data-driven/machine-learning-based models (mainly based on data, without any a priori knowledge).<sup>[44–47]</sup>

However, we consider that among all of them, the semiempirical models are the best option for analyses such as those performed in this work in terms of complexity, computational burden, real-time response, and reliability trade-off.<sup>[48]</sup> In this way, the present study uses semiempirical models for both LFP and NMC cells. Beltran et al.<sup>[41]</sup> provided a detailed description of such models corresponding to VL30P cells by SAFT and to JH3 cells by LG Chem, respectively. These models are selected for this study as mainstream examples of LFP and NMC commercial Li-ion cells widely adopted in battery packs installed in renewable applications. Both models, for LFP and NMC cells and summarized by Equation (1)–(4), analyze the capacity fade of the cells associated with either the calendar ( $C_{fade\_cal}$ ) or the cycling aging ( $C_{fade\_cyc}$ ). The former aging is mainly due to stress factors such as temperature and average state-of-charge (SOC) during stand-by periods, while the latter is strongly associated with the temperature of the cells under operation and with the number, C-rate, depth of discharge, and the average SOC of the cycles.

$$C_{fade\_cal\_LFP} = \alpha_{cal\_LFP} \cdot e^{\beta_{cal} \cdot T} \cdot t^{0.5} \quad (1)$$

$$C_{fade\_cyc\_LFP} = \alpha_{cyc\_LFP} \cdot e^{\beta_{cyc} \cdot T} \cdot NC^{0.5} \quad (2)$$

$$C_{fade\_cal\_NMC} = \alpha_{cal\_NMC} \cdot (V - 3.15) \cdot e^{-\frac{6976}{T}} \cdot t^{0.75} \quad (3)$$

$$C_{\text{fade}_{\text{cyc\_NMC}}} = \alpha_{\text{cyc\_NMC}} \cdot (1.8 \cdot (OV - 3.667)^2 + \Delta DOD + 0.1862) \cdot Q^{0.5} \quad (4)$$

where  $T$  is the temperature (in K),  $t$  is the time (in months for LFP, in days for NMC), NC represents the number of equivalent full cycles performed,  $V$  is the average daily voltage (in V),  $Q$  stands for the experienced charge throughput (in Ah),  $OV$  is the average voltage for each cycle (in V), and  $\Delta DOD$  is the depth of discharge of the cycle (in range of 0–1). Beltran et al.<sup>[41]</sup> provided the value of the different parameters  $\alpha_{\text{cal\_LFP}}$ ,  $\beta_{\text{cal}}$ ,  $\alpha_{\text{cyc\_LFP}}$ ,  $\beta_{\text{cyc}}$ ,  $\alpha_{\text{cal\_NMC}}$ , and  $\alpha_{\text{cyc\_NMC}}$ .

Therefore, the present study makes use of the results of the simulated annual operation of the hybrid power plant to feed these degradation models with the annual evolution of the corresponding variables ( $T$ ,  $t$ , NC,  $V$ ,  $Q$ ,  $OV$ , and  $\Delta DOD$ ). This provides a battery aging prognosis as a function of the electricity market structure considered for the plant operation.

### 3. Control Methodology to Firm the PV Plant Production with Batteries

Capacity firming is widely accepted as the capability to transform the intermittent power output from a renewable power generation plant, such as wind or solar PV, into a dispatchable power production that can be maintained at a committed level for a period of time.

Energy storage systems, mainly in the form of Li-ion batteries, have become a key player that allows firming the production of PV plants, acting as an energy buffer. In this way, BESS helps smoothing the PV output or even granting it to be constant by periods (minutes to hours) so that power commitments previously traded in the electricity markets are matched. The power exchanged with the grid is shaped by the combination of the power exchanged by the BESS and the PV production

$$P_{\text{grid}}(t) = P_{\text{PV}}(t) + P_{\text{BESS}}(t) \quad (5)$$

where  $P_{\text{grid}}(t)$  represents the instantaneous power exchanged with the grid (ideally, the one committed),  $P_{\text{PV}}(t)$  is the PV production, and  $P_{\text{BESS}}(t)$  is the power exchanged by the batteries. Depending on the operating framework (of those existing in the XBID continuous intraday market) where the hybrid plant is located (1 h, 30 min, or 15 min products), different constant-by-periods power sequences are required to firm the production. These power sequences range from 24 to up to 96 different values to be defined every day. Moreover, there is a lead time for the commitment of these power sequences that also depends on the intraday market in which the plant is participating. Ideally, if the lead time were equal to zero and the PV production forecast was assumed to be perfect, the optimized operation that would be targeted with a plant of this kind would be the one represented in **Figure 2** for the three possible operating frameworks: 1 h, 30 min, and 15 min energy products. Note how the power sequences tend to match the PV production and that the shorter the energy product, the closer the SOC is to the 50% reference value. Unfortunately, the market configuration always imposes a nonzero lead time when the exact

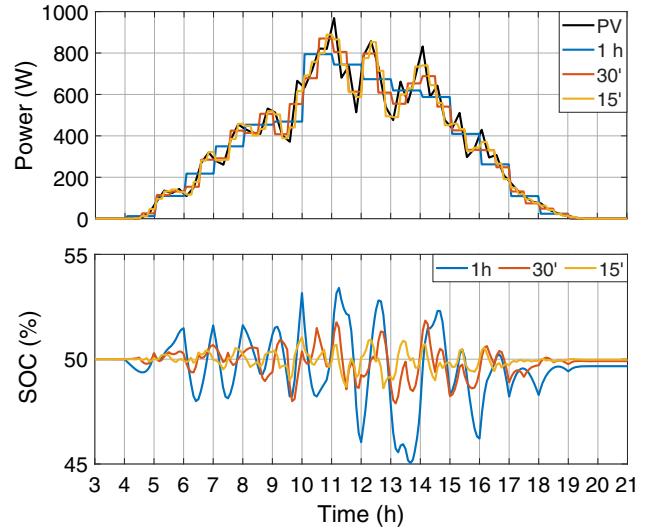


**Figure 2.** Optimal production power steps to be committed for different energy products and lead times of 30 min.

future irradiance (and the corresponding actual PV production) is not known in advance. This implies using a prediction model for  $P_{\text{PV}}$ .

In this sense, the methodology shown in **Figure 3** is proposed in this work. An irradiance forecasting tool predicts the future PV production, which is used, together with the actual SOC measurement, to calculate the optimal power sequence to be committed by means of an optimization problem. Next, a receding horizon strategy is carried out. This solely implements the first value of the calculated power sequence. Furthermore, **Figure 3** also shows the simulation procedure which has been used in this work for the simulation and assessment of the results that will be discussed in Section 4.3.

This optimization problem and the irradiance forecasting tool that have been implemented are introduced in the following, together with an example of the resulting plant operation with power commitments.

#### 3.1. Operational Optimization

In order to determine the constant-by-periods power sequences in the real context, in this work we propose an optimization problem which periodically minimizes the quadratic distance from the SOC of the BESS to a reference value (typically 50%) for the different settlement/lead time scenarios, without violating power and energy constraints. Each time instant  $t_0$  in which the optimization problem is cast, the SOC of the BESS is measured ( $E_{\text{ES}}(t_0)$ , in kWh) and the PV production forecast is updated based on the irradiance model introduced in Section 3.2. In this way, the successive optimization problems (6) are formulated using the most recent SOC measurement and meteorological information.

$$J = \min_{P_{\text{grid}}} \sum_{t=t_1}^{288} (\text{SOC}(t) - \text{SOC}_{\text{ref}})^2 \quad (6)$$

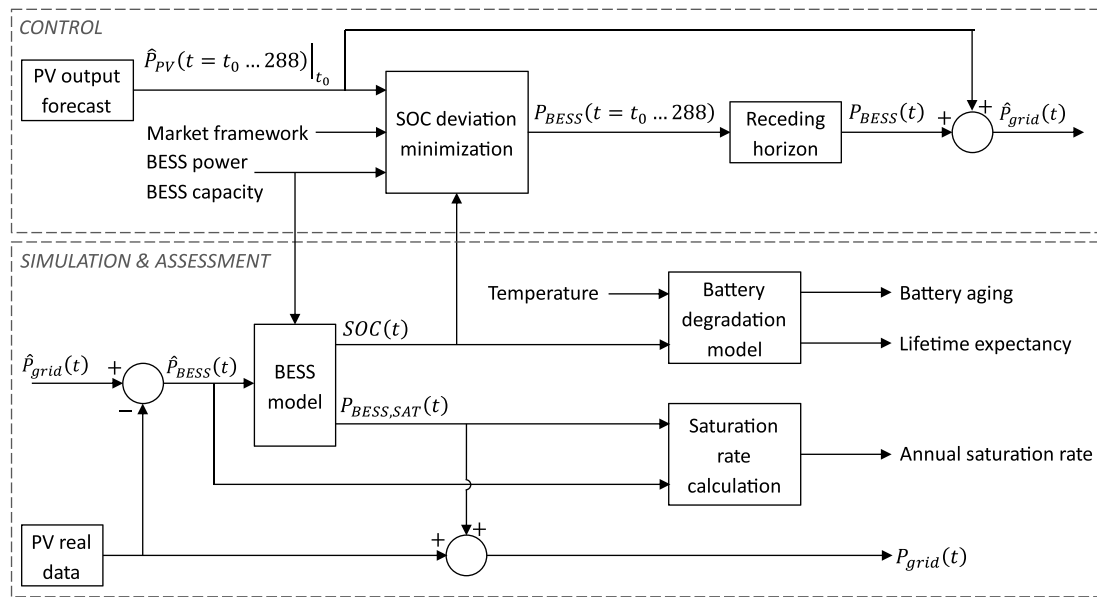


**Figure 3.** Process diagram of control and simulation workflows.

subject for  $t = t_0 \dots 288$  to

$$P_{grid}(t) = \begin{cases} p_{k,prev}, & t = t_0 \dots t_1 \\ p_{k+1}, & t = t_1 \dots t_1 + n \\ p_{k+2}, & t = t_1 + n + 1 \dots t_1 + 2n \\ \vdots & \\ p_N, & t = 289 - n \dots 288 \end{cases} \quad (7)$$

$$P_{grid}(t) = \hat{P}_{PV}(t)|_{t_0} + P_{BESS}(t) \quad (8)$$

$$P_{min} < P_{BESS}(t) < P_{max} \quad (9)$$

$$E_{BESS}(t) = E_{BESS}(t-1) - T \cdot P_{BESS}(t) \quad (10)$$

$$E_{min} < E_{BESS}(t) < E_{max} \quad (11)$$

where  $N$  is the number of elements in the power sequence committed for a day;  $n = \frac{288}{N}$  is the number of samples in each power step (considering a sampling time of  $T = 5$  min);  $\hat{P}_{PV}(t)|_{t_0}$  stands for the PV forecast at time  $t$  with the information available at time  $t_0$ ;  $SOC(t) = E_{BESS}(t)/C_{bat}$  is the instantaneous SOC of the battery in pu;  $E_{BESS}(t)$  is the energy stored in the battery (kWh);  $C_{bat}$  is its rated energy capacity (kWh);  $SOC_{ref}$  is the reference SOC;  $p_1 \dots p_N$  are the  $N$  constant power values;  $P_{min}$  and  $P_{max}$  are the rated power limits that the battery can provide; and  $E_{min}$  and  $E_{max}$  are the limit values for the energy stored in the battery. Note that both the summation in the objective function and the constraints consider 288 samples because of the aforementioned 5 min sample time.

As the optimization runs many times a day, note how  $P_{grid}$  contains a first value,  $p_{k,prev}$ , that stands for the power commitment derived from a previous market session. This is not a decision variable but has to be considered for the SOC evolution. In fact, this is the reference power value to be produced during the already committed period comprehending from  $t_0$  to

$t_1 = t_0 + \text{lead time}$ , after which the power dispatch is rescheduled. Further details on this optimization can be found in the study by Beltran et al.<sup>[49]</sup>

### 3.2. Irradiance Forecasting Model

The proposed control methodology requires an accurate irradiance forecast in order to provide the best results. Forecasting methods perform differently depending on the required granularity (somehow associated to the electricity product traded in the market) and on the forecasting horizon (equally associated to the traded product and to the lead time of the market). For the operation of a PV power plant, both intraday and day-ahead forecasts are used. Forecasting techniques which use machine learning and satellite data are the best ones for intraday forecasting,<sup>[50]</sup> whereas numerical weather predictions (NWP) and ensemble methods have a higher performance for longer forecasting horizons.<sup>[51]</sup>

To estimate the PV production, our simulations use an irradiance forecast model which combines the best methods for each forecasting horizon. An NWP model is used for the day-ahead forecasts and a deep learning model for the intraday forecasts. Hence, the incorporated NWP forecasts are those from the European Centre for Medium-Range Weather Forecasts (ECMWF),<sup>[52]</sup> which are obtained every 12 h and have a 10 day forecasting horizon with 1 h time steps for the first 90 h. Forecast of the surface net solar radiation are obtained from the high-resolution forecast: Atmospheric Model high-resolution 10-day forecast (HRES), which has a spatial resolution of  $0.1^\circ$  for both latitude and longitude. Moreover, the DNN proposed in Pérez et al.<sup>[53]</sup> is used to obtain the intraday forecasts. This DNN uses as its main input the results from the Surface Insolation under Clear and Cloudy Skies algorithm,<sup>[54]</sup> which provides estimated irradiance images from satellite data around the target location. These data matrices, which cover the last two

and a half hours, go through five convolutional layers in order to detect patterns and features and perform a type of deep-learning-based cloud motion detection. The results from the convolutional layers are combined with two more inputs, the measured irradiance in the last two and a half hours and estimations of the irradiance at the top of the atmosphere covering the forecasting horizon. Then these data are fed into a group of three dense layers which calculate the final irradiance forecasts.

The DNN forecasting covers a 6 h horizon with 15 min time steps, matching the time steps of the irradiance estimations. These forecasts can be updated every 15 min to be periodically fed to the control optimization algorithm previously introduced. The DNN forecasts are combined with the NWP ones to cover the forecasting horizon required by the optimization and the final forecasts are interpolated to a 5 min resolution to match the time steps for the optimization. In this way, it always calculates the future production power steps to be renegotiated in the intraday market making use of the latest irradiance forecast available.

### 3.3. PV Plant with BESS Power Commitments

To illustrate how the proposed algorithm works, let us consider the different profiles for a single day shown in **Figure 4**. The operation of the plant is conceptually initiated by executing the irradiance forecasting model, described in Section 3.2, as close as possible to the next intraday session closing time. In Figure 4, the forecast profiles obtained at 07:30, 10:30, and 14:30 are shown as an example together with the actual PV production, but a different forecast would be obtained for each market session in which the plant participates (48 sessions in this case). With this information, along with the current SOC measurement, the optimization introduced in Section 3.1 is performed, which generates the power profiles to commit in the market and that are shown in the central part of the figure. Again, only three power step profiles (from 8:00, 11:00, and 15:00 until the end of the day) are represented, but there would be a different one for each market session. Note how these profiles

start half an hour later than the corresponding irradiance forecasts implying that, for the chosen example, the lead time is equal to 30 min. Note also how the power commitment profiles roughly track the irradiance forecasts previously shown, except for the first value of the sequence. This is so because the optimization algorithm, with this first step, tends to compensate for previous forecasting errors which have moved the SOC away from its reference value (namely 50%). Finally, the last part of Figure 4 shows the power sequence finally exchanged with the grid for the day. This sequence of power steps results from the composition of the first steps defined at each of the previous sequences (in a predictive-control-like receding horizon strategy).

## 4. Simulation of the Plant Operation and Results on Battery Degradation

### 4.1. Simulations Description and Setup

The annual operation of the PV plant with batteries, controlled by the proposed algorithms and according to the workflow shown in Figure 3, has been simulated with Matlab using a time step of 5 min. Every simulation step is initiated by defining the optimal power exchanges with the grid  $\hat{P}_{grid}(t)$ . Then, the actual PV production is subtracted to get the power reference for the BESS,  $\hat{P}_{BESS}(t)$ . This is, in turn, used as the input to the BESS model. This checks if the power exchange is feasible (i.e., if the BESS is not saturated) and outputs both the actual power value applied  $P_{BESS,sat}(t)$  (which may be different if the input is not feasible) and the actual SOC. After that, the  $P_{BESS,sat}(t)$  value is added to the actual PV production to define the power actually exchanged with the grid,  $P_{grid}(t)$ .

After 1 year, the simulation algorithm returns evolution curves for three parameters: the  $P_{BESS,sat}(t)$ , the  $\hat{P}_{BESS}(t)$ , and the SOC. The two first are compared to define the annual saturation rate, while the latter allows to define the battery aging.

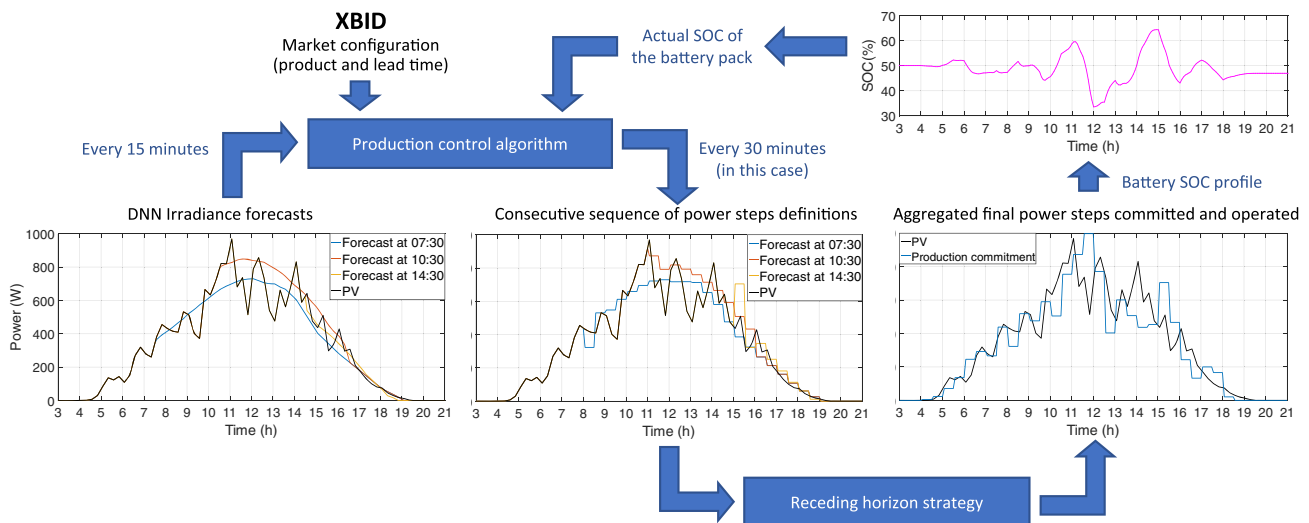


**Figure 4.** Schema of the control and operation methodology implemented for the capacity firming of PV plants with batteries.

For the case of the battery degradation analysis, this SOC evolution is introduced together with the operation temperature. The temperature conditions are assumed to be the same for the three sites because the battery packs installed in such hybrid plants are usually placed within containers including internal temperature regulation. In this way, the inner ambient temperature within the container is treated to be controlled between 20 and 25 °C throughout the year, varying within this range in agreement with the outer temperature, and limited to 20 or 25 °C when the outer temperature rises above or goes below those limits, respectively. Then, the container temperature is assigned to the Li-ion cells at rest, while a temperature offset of 20 °C is added to the batteries during operation (with temperature transients after turning on and off). Based on these parameters, the aging models provide the calculated calendar and cycling aging prognosis and we determine the battery lifetime expectancy till the end-of-life (EOL) of the batteries. This EOL is defined as the moment when the retained capacity equals a given percentage of its initial value, being 70% in this case (according to the warranty provided by SAFT and LG Chem for their cells).

These annual simulations are run at three European locations: a Mediterranean site close to València (Spain), a site close to Paris (France), and a site close to Amsterdam (The Netherlands). These locations present 1759, 1194, and 1077 peak sun-hours per year, respectively, and they are representative for three different climatic regions with varying characteristics in their PV production patterns. This selection aims at covering a wide range of production profiles for PV plants operated within XBID.

For each of these locations, simulations use actual irradiance values and comprehend four different battery sizes (ranging from 5 min to 1 h in equivalent accumulation time at rated power) and up to five XBID market structures (hour products with lead times of 1 h, and both 30 and 5 min, and half-hour and quarter-hour products with lead times of 30 min).

In this context, the analysis has initially focused on determining how well the hybrid plant can grant capacity firming throughout the year with the control operation system proposed for the different battery sizes at the various market structures. Then, for those battery sizes that would optimize the operation without involving large cost overruns, this work analyzes the influence of the intraday electricity market structure on their degradation, based on the two commercial battery packs introduced. Finally, it

provides a lifetime expectancy prognosis. Results on both extremes are introduced in the following.

#### 4.2. Results on Battery Sizes Required for Capacity Firming

The evolution of the SOC produced by the simulations allows us to identify when the hybrid power plant grants its production to the committed levels and when the battery gets saturated (i.e., it becomes completely charged or discharged). Table 1 summarizes, for each of the three analyzed locations, the percentage of time in a year in which the plant incurs deviations from the energy committed in the different intraday market structures.

The three locations return equivalent results regardless of their climatic conditions. Therefore, the site irradiance pattern does not significantly rule the battery size requirements. This is due to the proposed optimization strategy, which makes BESS capacity requirements to depend on the error between real production and the prediction instead of depending on the levels of irradiance. As the solar forecasting DNN performs with high accuracy at any location, it minimizes the impact of the solar pattern and variability on the battery degradation. On the contrary, it is strongly influenced by the market structure, where two characteristics highlight in this sense: the “product type” and the “lead time.” Note in Table 1 how the shorter the product and the closer the lead time, the lower is the percentage of time with deviations. For instance, if half-hour and quarter-hour products with a BESS energy capacity of 30 min are compared for the Amsterdam PV plant, the saturation value for the half-hour product case is twice as big as the one for the quarter-product market. In addition, the results for a BESS energy capacity of 5 min at the three locations are approximately two times bigger for a structure market with 1 h of lead time than for 5 min of lead time. Hence, a smaller battery is required to grant capacity firming. This is due to the proposed optimization strategy and to the use of the DNN-based high-performing short-term forecasting tool, which achieves better results with shorter time elapsed from auction closing time to starting delivery. Therefore, it can be concluded that BESS energy capacities of 1 h will completely grant PV firming while 30 and 15 min batteries will achieve it more than 95% of the time. Only the case of 5 min capacity batteries would produce deviations beyond the 10% of the operation time. Although not

**Table 1.** BESS annual saturation rate for the intraday market structures considered (in %).

Product	Lead time	Paris				Valencia				Amsterdam			
		BESS capacity				BESS capacity				BESS capacity			
		1 h	30'	15'	5'	1 h	30'	15'	5'	1 h	30'	15'	5'
15'	30'	0	0.2	1.4	9	0	0.2	1.5	8.8	0	0.1	0.9	9.8
30'	30'	0	0.4	2.4	11.9	0	0.5	2.4	11.8	0	0.2	1.8	13.4
1 h	1 h	0.3	1.6	5.4	19.4	0.2	1.7	5.4	19.7	0.1	1.0	5.3	19.6
1 h	30'	0.1	0.7	3.2	16	0.1	0.8	3.5	15.6	0	0.3	2.7	16.2
1 h	5'	0	0.3	1.9	11.2	0	0.4	2.1	11.5	0	0.1	1.3	12.1

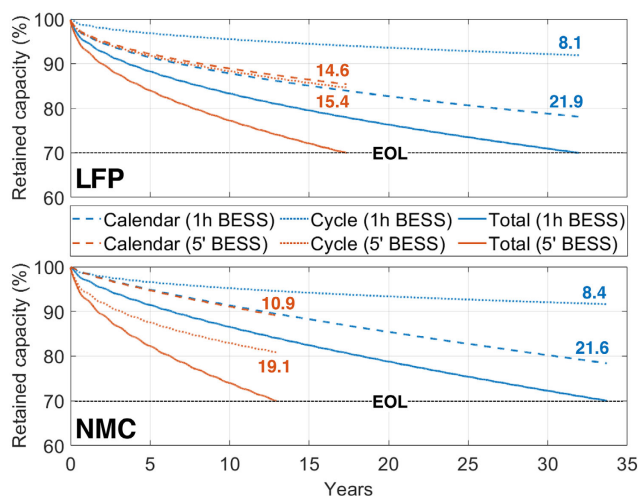


**Figure 5.** Total degradation and partial calendar and cycle aging experienced by a 1 h (blue) and a 5 min (red) capacity LFP (top) and NMC (down) battery packs.

so good in terms of PV capacity firming purposes, these are also included in the aging analysis because of their significantly smaller CAPEX.

### 4.3. Degradation Results and Lifetime Expectancy

The degradation analysis experienced by the indicated two types of commercial battery packs is based on the annual operation conditions. These are extracted from the SOC (cycling activity defined by the control algorithm and the market configuration) returned by the simulations and from the temperature vector (calendar activity) registered at each of the locations.

**Figure 5** exhibits the capacity degradation experienced in Paris by four different battery packs when providing 30 min products. The two battery packs represented in the upper graph correspond to commercial LFP cells from SAFT and present initial energy capacities of 1 h (blue lines) and 5 min (red lines). The two represented in the lower graph belong to NMC commercial cells from LG Chem and present the same initial capacities (1 h and 5 min with the corresponding reference colors).

Observe how for both types of cells, smaller capacity packs present lifetime expectancy values much shorter (around 17 and 13 years, respectively) than larger packs (up to 32 and

33 years, respectively). Although results are quite different among them, such high lifetime expectancy values (all of them beyond 10 years) are considered particularly good projections. These are mainly achieved because of two reasons: first, the PV capacity firming application is concluded to be not very stressing in terms of battery use (low cycle aging) and, second, the importance provided to the calendar aging in the corresponding degradation models defined in (1) to (4). In this regard, note how the calendar effect is minimized in this application due to the control of the ambient temperature during operation. Although calendar aging has been disregarded in some degradation studies, it presents a clear weight in these cells' models even in the case of temperature-controlled operation. In fact, if the partial effect of the calendar is compared to that of the cycle aging for each cell type in Figure 5, note how it cannot be overlooked at all. Considering the maximum degradation value defined by manufacturers to achieve the EOL of the battery pack, 30% (i.e., retained capacity of 70%), the calendar may weight from 36% out of that maximum for the NMC 5 min battery pack to around 73% for the LFP 1 h battery pack. In the same way, notice how the cycle aging influence is significantly higher in both chemistries for the 5 min battery packs (around 50% and 64%, respectively). This is because the limited energy capacity of these packs forces them to operate and cycle more frequently. Also, the experienced cycles will be deeper with respect to the rated capacity, which increases the degradation.

**Table 2 and 3** introduce a complete summary of the lifetime expectancy values that both types of Li-ion battery packs will present at each of the three locations. Note that all the considered combinations (energy capacities according to the battery sizes discussed in Section 4.2 and intraday market structures) are gathered for each of the chemistries. As for the deviation results presented in Section 4.2, results on lifetime expectancy show that the irradiance patterns experienced in the considered locations do not significantly influence the battery degradation. Therefore, the aging analysis introduced here would be valid for any location within the XBID context as long as the battery packs are kept under temperature-controlled conditions. Also, the comparison of the lifetime expectancy values represented in both tables leads to the conclusion that the two battery packs present similar responses in terms of aging. Both models seem to deal similarly with the stress factors and none of them could be sentenced to be clearly superior in this regard. On the contrary, it is important to point out the varying degradation they experience depending on both the energy product provided by the hybrid

**Table 2.** Lifetime expectancy of LFP battery packs (in years).

Product	Lead time	Paris				Valencia				Amsterdam			
		BESS capacity				BESS capacity				BESS capacity			
		1 h	30'	15'	5'	1 h	30'	15'	5'	1 h	30'	15'	5'
15'	30'	38.8	28.4	20.2	14.4	38.7	28.9	21.2	15.4	39.4	28.5	19.6	13.8
30'	30'	36.6	26.8	20.3	15.8	36.8	27.8	21.3	16.4	39.6	27.2	19.5	15.5
1 h	1 h	32	24.3	19.5	17.4	32.2	24.7	19.8	17.4	32.5	23.5	18.8	17.4
1 h	30'	35	26.1	20.2	16.5	34.7	26.6	20.6	16.5	36.1	26.2	19.4	16.4
1 h	5'	38.1	28.4	21.2	15.8	37.7	28.6	21.6	15.8	39.6	29.3	20.8	15.8



**Table 3.** Lifetime expectancy of NMC battery packs (in years).

Product	Lead time	Paris				Valencia				Amsterdam			
		BESS capacity				BESS capacity				BESS capacity			
		1 h	30'	15'	5'	1 h	30'	15'	5'	1 h	30'	15'	5'
15'	30'	39.5	30.1	20.3	12.2	39.2	30.4	21.4	13.3	39.8	30.2	19.6	11.3
30'	30'	37.7	28	19.6	12.7	37.7	29.2	21.1	13.6	40.1	28.3	18.5	12.1
1 h	1 h	33.7	24.9	18.1	12.9	34.1	25.8	19	13	33.9	23.7	16.8	13
1 h	30'	36.4	27.2	19.4	12.6	36.2	28.1	20.4	13.3	37	26.8	18	12.5
1 h	5'	39	29.7	21.1	12.7	38.6	30.4	22	13.3	40.1	30.5	20.4	12.6

plant and the lead time defined by the market. In this regard, check how the shorter the product and the closer the lead time, the better the battery performs avoiding certain degradation, except for the case of the 5 min battery packs. For this size of battery, the operation saturates the battery significantly throughout the year, which distorts the results. Then, in general, it will be always better for the sake of the batteries lifetime to operate the plant in a market with 15 min products with lead times of 30 min or 1 h products with lead times of 5 min, rather than in a 1 h product market with lead times of 1 h (being the latter the common structure for the cross-border exchanges). Finally, the sizing can be concluded again as a strong influencing factor because results demonstrate that the smaller the battery size, the significantly shorter the lifetime expectancy becomes for all the combinations and locations analyzed.

Then, both battery pack size and market structure are identified as the main factors somehow conditioning the battery pack lifetime expectancy. Considering the location independence and the similitude between the commercial battery models analyzed, an accurate evaluation on potential economic benefits achievable at each market has to be conducted to define the optimal size (and the corresponding cost overrun) to be installed at any given PV plant.

## 5. Conclusions

This work aimed at analyzing the degradation experienced by two of the most widely used types of Li-ion batteries (NMC and LFP) installed to qualify PV plants with capacity firming to trade at different intraday electricity markets. In this framework, the influence of the intraday market structure on the degradation record of differently sized batteries was studied by means of simulations at three European locations.

To estimate the PV production, these simulations used an irradiance forecasting model that combined a deep learning approach with ECMWF derived forecasts. Also, a quadratic optimization control algorithm was implemented to generate the power commitments to be traded in the electricity market by the hybrid plant. Finally, semiempirical degradation models calibrated according to the warranty published for two current state-of-the-art commercial battery packs have been adopted.

According to the resulting values, the proposed control strategy allowed to decouple the saturation rate for a given BESS size from the climatic conditions imposed by the location

of the plant. Therefore, the saturation became mainly dependent on the PV forecast error, but with little effect due to its low value in the three locations under study, and on the intraday market structure (energy product and lead time). Annual saturation rate results varied from values around zero for 1 h battery capacities to percentages between 9% and 20% for 5 min capacities.

Regarding battery degradation, both battery chemistry and location of the plant were factors with little influence. On the contrary, the degradation experienced by the BESS varied significantly with its energy capacity and the intraday market structure (energy product and lead time). In this sense, trading in continuous intraday markets with shorter settlement periods, as well as taking advantage of closer lead times, allowed reducing the degradation by around 5–20% and increasing the lifetime expectancy up to 7 years, depending on the implemented battery size. The simulations also showed that calendar aging cannot be disregarded even under the temperature-controlled conditions of the study.

## Acknowledgements

The authors would like to thank the financial support provided by the Universitat Jaume I from Castelló (Spain), the Generalitat Valenciana (GV), and the European Social Fund (ESF). This work was developed within the context of projects UJI-B2021-35, GV-2019-087, and grant numbers ACIF/2019/106 and PREDOC/2020/35.

## Conflict of Interest

The authors declare no conflict of interest.

## Data Availability Statement

Research data are not shared.

## Keywords

electricity markets, lifetime expectancy, lithium-ion batteries, photovoltaic (PV) capacity firming

Received: October 26, 2021

Revised: February 28, 2022

Published online:

- [1] REN21, *Renewables 2020 Global Status Report*, Technical report, REN21, Paris **2020**.
- [2] IRENA, *Adapting Market Design to High Shares of Variable Renewable Energy*, Technical report, International Renewable Energy Agency (IRENA), Abu Dhabi **2017**.
- [3] BloombergNEF, *Electric Vehicle Outlook 2020*, Technical report, BloombergNEF, London, UK **2020**.
- [4] M. Raugei, E. Leccisi, V. M. Fthenakis, *Energy Technol.* **2020**, *8*, 1901146.
- [5] Lazard, *Levelized Cost of Storage Analysis—Version 7.0*, <https://www.lazard.com/media/451882/lazards-levelized-cost-of-storage-version-70-vf.pdf> (accessed: October 2021).
- [6] A. Bhattacharjee, H. Samanta, A. Ghosh, T. K. Mallick, S. Sengupta, H. Saha, *Energy Technol.* **2021**, *9*, 2100199.
- [7] U. S. Energy Information Administration (EIA), *Battery Storage in the United States: An Update on Market Trends*, U. S. Energy Information Administration (EIA), Washington DC, USA **2021**.
- [8] ENTSO-E, *The Platform for the International Coordination of Automatic Frequency Restoration and Stable System Operation (PICASSO)*, [https://www.entsoe.eu/network\\_codes/eb/picasso/](https://www.entsoe.eu/network_codes/eb/picasso/) (accessed: March 2022).
- [9] ENTSO-E, *Manually Activated Reserves Initiative (MARI)*, [https://www.entsoe.eu/network\\_codes/eb/mari/](https://www.entsoe.eu/network_codes/eb/mari/) (accessed: March 2022).
- [10] European Commission, *The Recovery and Resilience Facility*, [https://ec.europa.eu/info/business-economy-euro/recovery-coronavirus/recovery-and-resilience-facility\\_en](https://ec.europa.eu/info/business-economy-euro/recovery-coronavirus/recovery-and-resilience-facility_en) (accessed: March 2022).
- [11] Y. Yang, S. Bremner, C. Menictas, M. Kay, *Renewable Sustainable Energy Rev.* **2018**, *91*, 109.
- [12] R. V. Monteiro, G. C. Guimarães, F. A. Moura, M. R. Albertini, F. B. Silva, *Electric Power Syst. Res.* **2017**, *144*, 163.
- [13] E. Nasrolahpour, S. J. Kazempour, H. Zareipour, W. D. Rosehart, *IEEE Trans. Sustainable Energy* **2016**, *7*, 1462.
- [14] H. Beltran, I. Tomas Garcia, J. C. Alfonso-Gil, E. Perez, *IEEE Trans. Energy Convers.* **2019**, *34*, 554.
- [15] A. Gonzalez-Garrido, A. Saez-de Ibarra, H. Gaztanaga, A. Milo, P. Eguia, *IEEE Trans. Power Syst.* **2019**, *34*, 5115.
- [16] U. Raveendrannair, M. Sandelic, A. Sangwongwanich, T. Dragicevic, R. Costa Castello, F. Blaabjerg, *IEEE Trans. Energy Convers.* **2021**, *36*, 2276.
- [17] M. S. ElNozahy, T. K. Abdel-Galil, M. M. Salama, *Electric Power Syst. Res.* **2015**, *125*, 55.
- [18] S. A. Abdelrazek, S. Kamalasadán, *IEEE Trans. Ind. Applic.* **2016**, *52*, 2607.
- [19] G. Wang, M. Ciobotaru, V. G. Agelidis, *IEEE Trans. Sustainable Energy* **2014**, *5*, 834.
- [20] M. Pantos, S. Riaz, A. C. Chapman, G. Verbic, in *2017 Australasian Universities Power Engineering Conference (AUPEC)*, IEEE, Piscataway, NJ **2017**.
- [21] H.-T. Yang, C.-M. Huang, Y.-C. Huang, Y.-S. Pai, *IEEE Trans. Sustainable Energy* **2014**, *5*, 917.
- [22] H. Beltran, E. Perez, N. Aparicio, P. Rodriguez, *IEEE Trans. Sustainable Energy* **2013**, *4*, 474.
- [23] M. Swierczynski, D. I. Stroe, A.-I. Stan, R. Teodorescu, D. U. Sauer, *IEEE Trans. Sustainable Energy* **2014**, *5*, 90.
- [24] M. R. Sarker, M. D. Murbach, D. T. Schwartz, M. A. Ortega-Vazquez, *Electric Power Syst. Res.* **2017**, *152*, 342.
- [25] F. Berglund, S. Zaferanlouei, M. Korpas, K. Uhlen, *Energies* **2019**, *12*, 4450.
- [26] S. Abdelrazek, S. Kamalasadán, *IEEE Trans. Ind. Applic.* **2016**, *52*, 5175.
- [27] S. Abdelrazek, S. Kamalasadán, J. Enslin, T. Fenimore, in *2015 IEEE Energy Conversion Congress and Exposition (ECCE)*, IEEE, Piscataway, NJ **2015**, pp. 62–69.
- [28] US Federal Energy Regulatory Commission, 81 FR 86522 - Electric Storage Participation in Markets Operated by Regional Transmission Organizations and Independent System Operators DOE, Washington DC **2016**, p. 139 <https://www.govinfo.gov/app/details/FR-2016-11-30/2016-28194/summary> (accessed: March 2022).
- [29] N. E. Koltsaklis, A. S. Dagoumas, *Appl. Energy* **2018**, *231*, 235.
- [30] F. Ocker, V. Jaenisch, *Energy Policy* **2020**, *145*, 111731.
- [31] P. Ayuso, H. Beltran, J. Segarra-Tamarit, E. Pérez, *Math. Comput. Simulation* **2021**, *183*, 97.
- [32] D. Roman, S. Saxena, V. Robu, M. Pecht, D. Flynn, *Nat. Mach. Intell.* **2021**, *3*, 447.
- [33] M. Berecibar, I. Gandiaga, I. Villarreal, N. Omar, J. Van Mierlo, P. Van den Bossche, *Renewable Sustainable Energy Rev.* **2016**, *56*, 572.
- [34] N. G. Panwar, S. Singh, A. Garg, A. K. Gupta, L. Gao, *Energy Technol.* **2021**, *9*, 2000984.
- [35] A. Barré, B. Deguilhem, S. Grolleau, M. Gérard, F. Suard, D. Riu, *J. Power Sources* **2013**, *241*, 680.
- [36] K. K. Sadabadi, X. Jin, G. Rizzoni, *J. Power Sources* **2021**, *481*, 228861.
- [37] Y. Gao, K. Liu, C. Zhu, X. Zhang, D. Zhang, *IEEE Trans. Ind. Electron.* **2022**, *69*, 2684.
- [38] X. Hu, S. Li, H. Peng, *J. Power Sources* **2012**, *198*, 359.
- [39] T. Feng, L. Yang, X. Zhao, H. Zhang, J. Qiang, *J. Power Sources* **2015**, *281*, 192.
- [40] D. Andre, M. Meiler, K. Steiner, H. Walz, T. Soczka-Guth, D. Sauer, *J. Power Sources* **2011**, *196*, 5349.
- [41] H. Beltran, P. Ayuso, E. Pérez, *Energies* **2020**, *13*, 568.
- [42] S. Hong, T. Yue, H. Liu, *Int. J. Intell. Syst.* **2020**.
- [43] J. Schmalstieg, S. Käbitz, M. Ecker, D. U. Sauer, *J. Power Sources* **2014**, *257*, 325.
- [44] L. Ren, L. Zhao, S. Hong, S. Zhao, H. Wang, L. Zhang, *IEEE Access* **2018**, *6*, 50587.
- [45] K. A. Severson, P. M. Attia, N. Jin, N. Perkins, B. Jiang, Z. Yang, M. H. Chen, M. Aykol, P. K. Herring, D. Fraggedakis, M. Z. Bazant, S. J. Harris, W. C. Chueh, R. D. Braatz, *Nat. Energy* **2019**, *4*, 383.
- [46] X. Hu, J. Jiang, D. Cao, B. Egardt, *IEEE Trans. Ind. Electron.* **2015**, *63*, 2645.
- [47] V. Klass, M. Behm, G. Lindbergh, *J. Power Sources* **2014**, *270*, 262.
- [48] I. Baghdadi, O. Briat, J.-Y. Delétage, P. Gyan, J.-M. Vinassa, *J. Power Sources* **2016**, *325*, 273.
- [49] H. Beltran, J. Cardo-Miota, J. Segarra-Tamarit, E. Pérez, *J. Energy Storage* **2021**, *33*, 102036.
- [50] C. Voyant, G. Notton, S. Kalogirou, M.-L. Nivet, C. Paoli, F. Motte, A. Fouilloy, *Renewable Energy* **2017**, *105*, 569.
- [51] R. Blaga, A. Sabadus, N. Stefu, C. Dughir, M. Paulescu, V. Badescu, *Progr. Energy Combust. Sci.* **2019**, *70*, 119.
- [52] F. Molteni, R. Buizza, T. Palmer, T. Petroliaigis, *Quart. J. R. Meteorol. Soc.* **1996**, *122*, 73.
- [53] E. Pérez, J. Pérez, J. Segarra-Tamarit, H. Beltran, *Solar Energy* **2021**, *218*, 652.
- [54] W. Greuell, J. F. Meirink, P. Wang, *J. Geophys. Res.: Atmos.* **2013**, *118*, 2340.
- [55] J. Verseille, S. Alaimo, *ENTSO-E*, **2018**.